**Cell Reports, Volume *34***

## Supplemental Information

# Large, Stable Spikes Exhibit Differential Broadening in Excitatory and Inhibitory Neocortical Boutons

**Andreas Ritzau-Jost, Timur Tsintsadze, Martin Krueger, Jonas Ader, Ingo Bechmann, Jens Eilers, Boris Barbour, Stephen M. Smith, and Stefan Hallermann**

# Supplemental Information

**Supplementary Figures 1–5:**

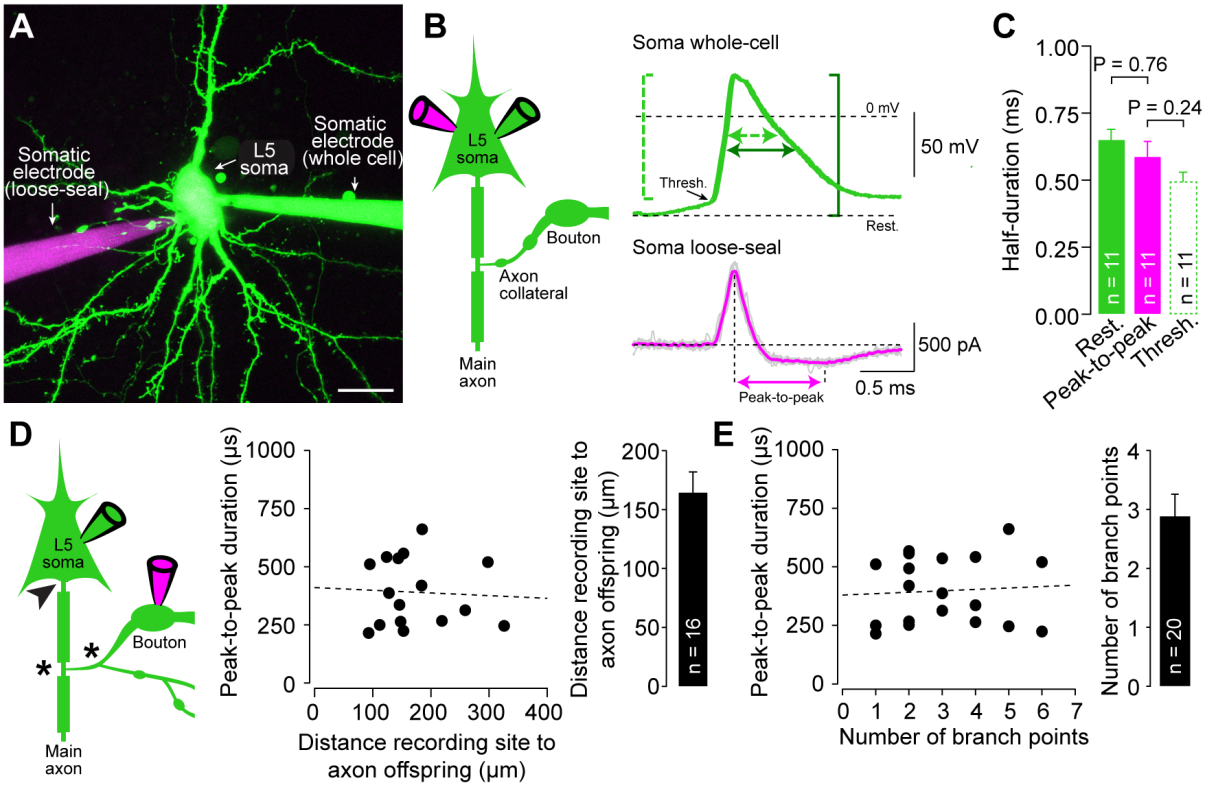


**Figure S1 Loose-seal recordings reliably reflect spike duration and indicate stable axonal spike propagation. Related to Figure 1.**

**(A)** 2P-image of a simultaneous somatic whole-cell (green pipette) and loose-seal recording (magenta pipette) from a neocortical layer 5 pyramidal neuron. Scale bar 15 µm, maximum z-projection of a stack of 69 images, z-step size 1 µm.

**(B)** *Left*: Pictogram of the recording configuration. *Right:* Overlay of 31 evoked somatic action potentials (green) in whole cell-mode and action potential-evoked somatic currents simultaneously recorded in loose-seal mode (magenta). Braket depict somatic action potential amplitude from pre-stimulus membrane potential (dark green) and action potential threshold (light green, broken line). Action potential half-durations at corresponding half-amplitudes (green arrows) and peak-to-peak duration in somatic loose-seal recording (magenta arrow) indicated.

**(C)** Half-duration of somatic action potentials quantified from pre-stimulus membrane potential and action potential threshold related to peak-to-peak duration of somatic currents recorded simultaneously in loose-seal mode (bar graphs as mean ± SEM, color code as in **B**, n indicates number individual paired somatic recordings).

**(D)** *Left*: Pictogram of a paired bouton-soma recording illustrating the offset of the axon proper from the soma (arrowhead) and axonal branch points between axon offset and bouton recording site (asterisks). *Middle*: Peak-to-peak duration of loose-seal recorded currents plotted versus distance between bouton recording site and axon offset (broken line as linear fit). *Right:* Distance of bouton recording site from axonal offset (bar graph as mean ± SEM, n indicates number of paired bouton-soma recordings).

**(E)** *Left:* Peak-to-peak current duration plotted versus number of axonal branch points between bouton recording site and axon offset (broken line as linear fit). *Middle:* Peak-to-peak duration of loose-seal recorded currents plotted versus branch point number between bouton recording site and axon offset (broken line as linear fit). *Right:* Branch point number between bouton recording site and axonal offset (bar graph as mean ± SEM, n indicates number of paired bouton-soma recordings).

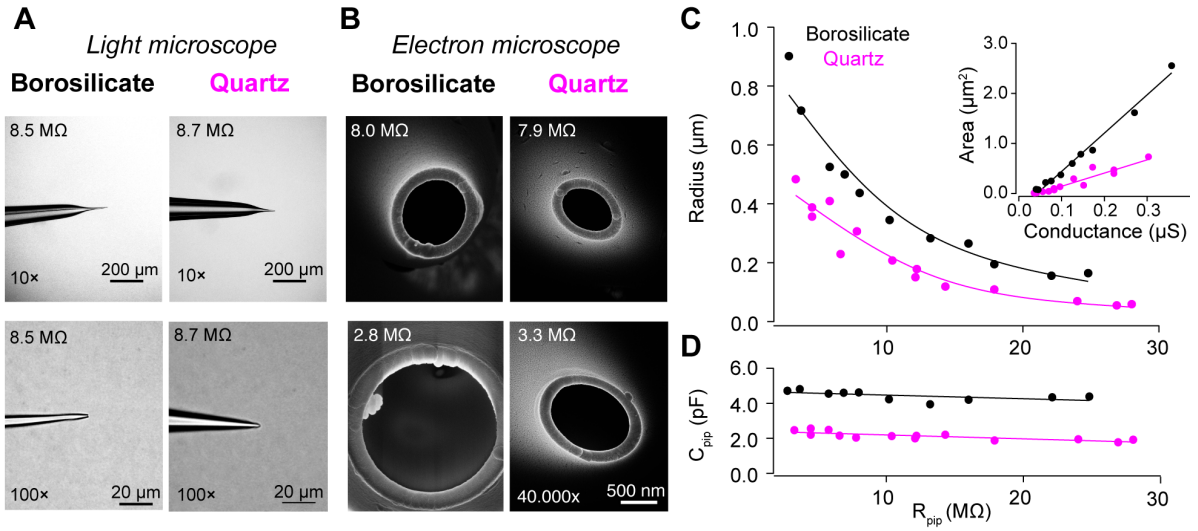


**Figure S2 Borosilicate and quartz glass pipettes show different geometrical and electrical properties. Related to Figure 2.**

**(A)** *Left:* Light microscopic images of example borosilicate pipettes at 10x and 100x magnification. *Right:* Light microscopic images of example quartz pipettes at same magnification.

**(B)** *Left:* Electron microscopic images of borosilicate glass pipette tips of various pipette resistances. *Right:* Electron microscopic images of quartz glass pipette tips.

**(C)** Radius of the tip opening for borosilicate and quartz glass pipettes (in black and magenta, respectively) of different pipette resistances. Solid lines are smoothed spline interpolations. Inset: Pipette tip opening area plotted versus pipette conductance superimposed with linear fits.

**(D)** Pipette capacitance of borosilicate and quartz glass pipettes (in black and magenta, respectively) of different pipette resistances. Solid lines are linear fits to pipette capacitance. Pipette resistances and capacitances were recorded from sister pipettes of those imaged by electron microscopy.

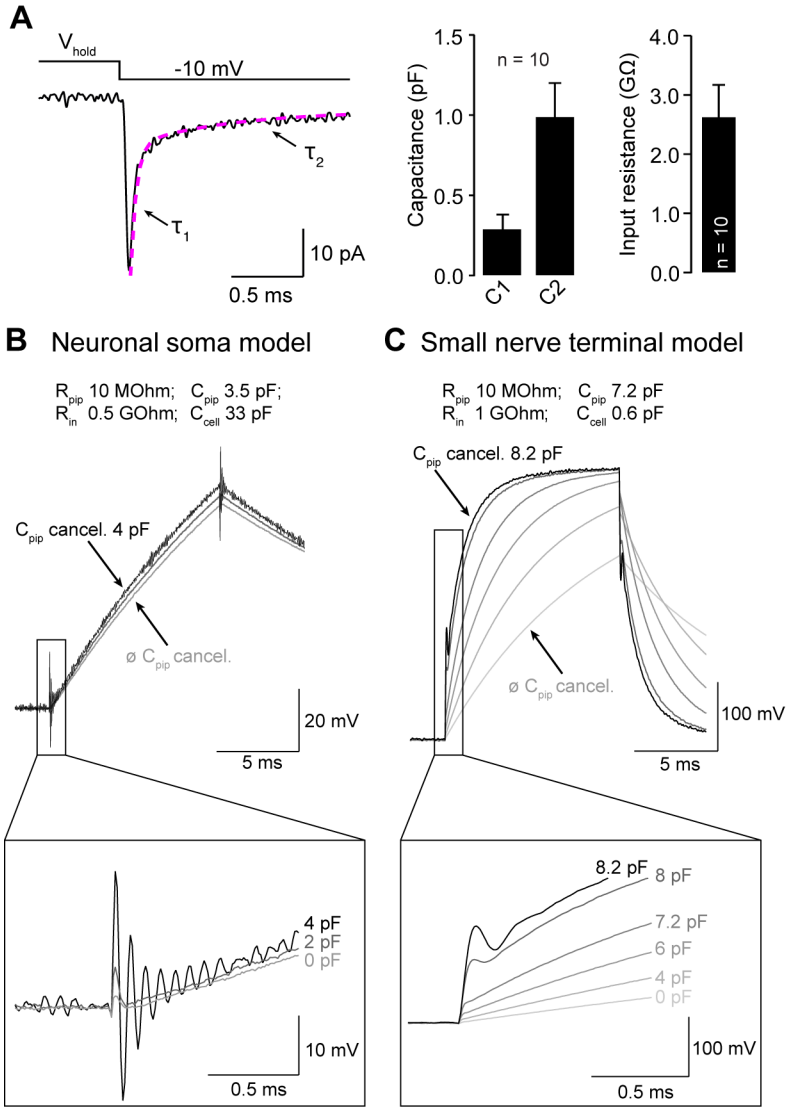


**Figure S3 The small capacitance of *en passant* boutons precludes conventional pipette capacitance determination in current-clamp mode. Related to Figure 3.**

**(A)** *Left:* Current obtained from the difference between current responses in cell-attached mode and immediately after establishing whole-cell mode from bouton recordings superimposed with a bi-exponential fit (magenta broken line). *Right:* Average derived passive parameters for boutons recordings (mean ± SEM).

**(B)** *Top:* Increasing pipette capacitance cancellation in current-clamp mode in a neuronal soma model circuit leads to voltage oscillations clearly separable from slower voltage changes of the somatic capacitance. *Bottom:* Expansion of the initial voltage change upon current injection for different pipette capacitance ($C_{pip}$) cancellations

**(C)** *Top:* Current injection-evoked voltage responses in the bouton model (same as in Figure 3) for different pipette capacitance cancellations. *Bottom:* Enlarged initial voltage change upon current injections.

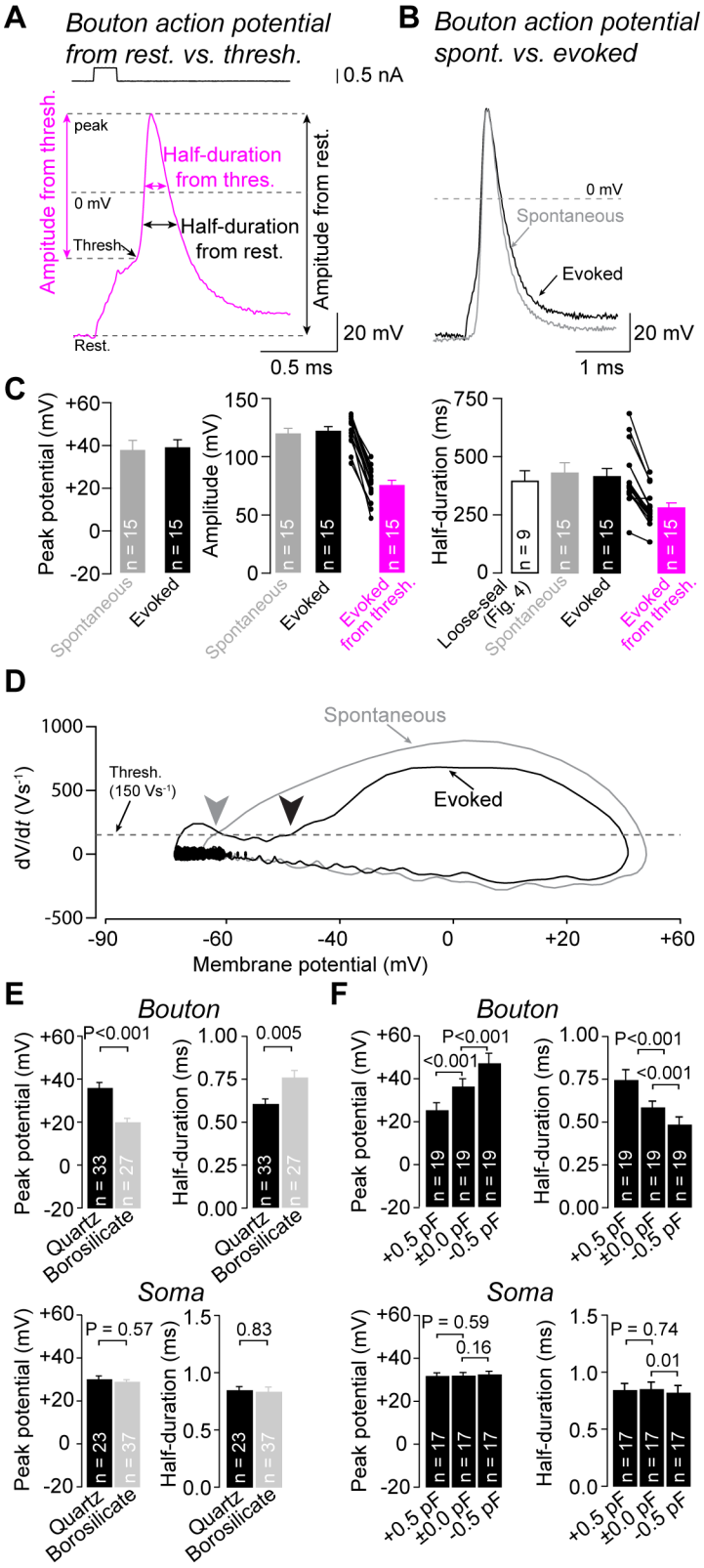


**Figure S4 Bouton action potentials are unperturbed by current-injection but strongly affected by absolute pipette capacitance and capacitance compensation. Related to Figure 5.**

**(A)** Illustration of action potential amplitude and half-duration quantified from pre-stimulus membrane potential (black) and action potential threshold (magenta) of a bouton action potential evoked by current injection with a quartz glass pipette in cultures.

**(B)** Overlay of example spontaneous (black) and evoked action potentials (grey) recorded from the same bouton with a quartz glass pipette in cultures. Action potentials were aligned to the action potential peak.

**(C)** *Left:* Peak potential of spontaneous and evoked action potentials. *Middle:* Amplitude of spontaneous and evoked action potentials. *Right:* Half-duration of spontaneous and evoked action potentials (bar graphs as mean ± SEM, n indicates the number of individual bouton recordings or paired bouton-soma recordings).

**(D)** Phase-plane plot of the evoked and spontaneous action potential shown in **B**. Voltage at which action potential threshold is crossed (defined as 150 $Vs^{-1}$) indicated by arrow heads (color code as in **B**).

**(E)** *Top:* Average peak potential and half-duration of action potentials recorded from boutons with quartz (black) or borosilicate glass pipettes (grey). *Bottom:* Average peak potential and half-duration of somatic action potentials recorded with quartz (black) or borosilicate glass pipettes (grey). All recordings with Multiclamp 700A amplifier (bar graphs as mean ± SEM).

**(F)** *Top:* Average peak potential and half-duration of action potentials in boutons when varying capacitance compensation (±0.5 pF). *Bottom:* Average peak potential and half-duration of somatic action potentials when varying capacitance compensation (±0.5 pF; bar graphs as mean ± SEM).

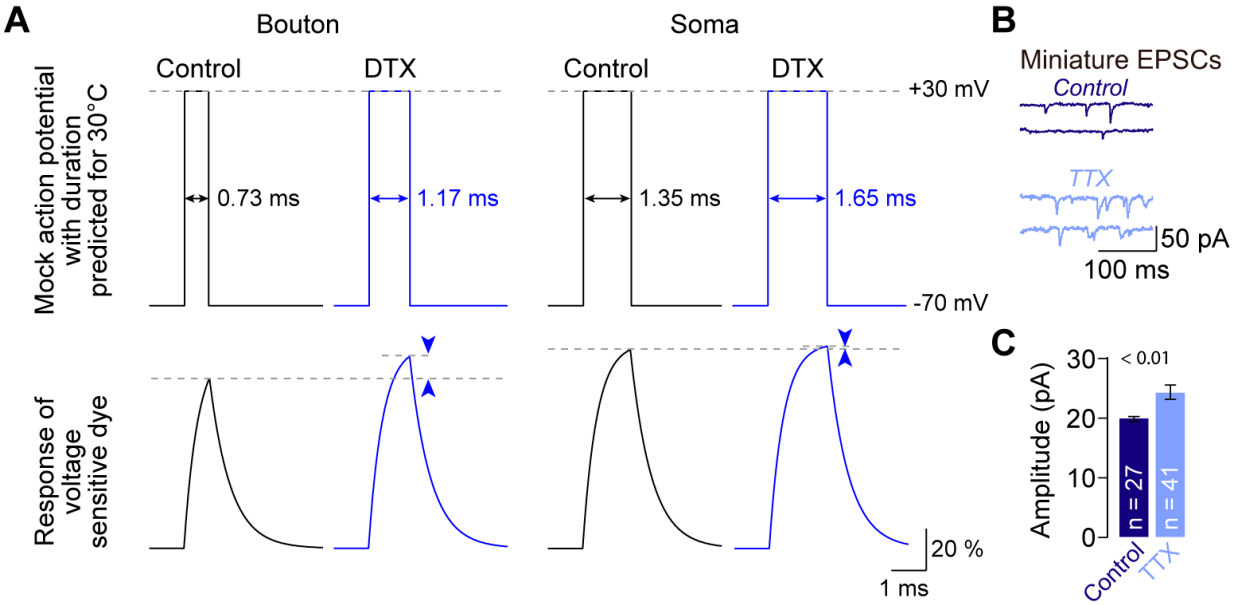


**Figure S5 Filtering of spike waveform imposed by voltage sensitive dye kinetics and scaling of postsynaptic miniature events by chronic activity blockade. Related to Figure 6.**

**(A)** Using genetically-encoded voltage sensors, Hoppa et al. (2014) reported small amplitudes of presynaptic action potentials in cultured hippocampal neurons that increase upon pharmacological blockade of $K_v$ channels (recordings at 30°C). Different methods of recording action potentials might account for the discrepancy with our results. To investigate the impact of the kinetics of the genetically encoded voltage sensitive dye, Mock action potentials (*top*) with durations predicted for 30°C from our data measured at 36 °C (assuming a $Q_{10}$ value of 2.2, see *Methods Details*) were used to calculate fluorescence response of the employed voltage sensitive dye (Archaerhodopsin, *bottom*) according to published on- and off-response rates (Bando et al., 2019; Maclaurin et al., 2013). The exponential rise and decay time constants were 0.4 and 0.6 ms for steps from -70 to +30 mV and from +30 to -70 mV, respectively. Broadening bouton action potentials (as occurring following potassium channel block; cf. Figure 6) permitted the voltage-sensor enough time to progress further towards steady-state and consequently increased the apparent fluorescence response by ~10 %. In contrast, the slower somatic action potential allowed the fluorescent signal more time to reach steady state and resulted in an apparently larger amplitude. Consequently, action potential broadening by DTX had minimal effect on the somatic fluorescence response or spike amplitude. Therefore, the reported small bouton action potential amplitude and the apparent regulation by potassium channels by Hoppa et al. (2014) might be explained by the slow kinetics of the employed voltage-sensor (Bando et al.,

2019; Maclaurin et al., 2013). Furthermore, the used sampling frequency by Hoppa et al. (2014) of 1 or 2 kHz might contribute to a limited temporal resolution.

**(B)** Example recordings of miniature excitatory postsynaptic currents (mEPSCs) in somatic recordings from cultured neurons under control conditions and after exposure of cultures to TTX (2 µM in culture medium for 48h prior to recordings).

**(C)** Mean mEPSC amplitude after exposure to TTX normalized to control conditions (n indicates number of individual somatic recordings; bar graphs as mean ± SEM).